BCSJ

Selected Paper

A Benzophosphole *P*-Oxide with an Electron-Donating Group at 3-Position: Enhanced Fluorescence in Polar Solvents

Eriko Yamaguchi,[1] Aiko Fukazawa,*[1] Youhei Kosaka,[1] Daisuke Yokogawa,[1,2] Stephan Irle,*[1,2] and Shigehiro Yamaguchi*[1,2]

[1]Department of Chemistry, Graduate School of Science, Nagoya University, Furo, Chikusa-ku, Nagoya, Aichi 464-8602

[2]Institute of Transformative Bio-molecules (WPI-ITbM), Nagoya University, Furo, Chikusa-ku, Nagoya, Aichi 464-8602

E-mail: yamaguchi@chem.nagoya-u.ac.jp

Received: July 9, 2015; Accepted: August 10, 2015; Web Released: August 18, 2015

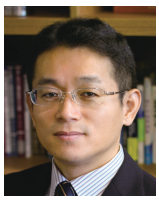

Shigehiro Yamaguchi

Shigehiro Yamaguchi received his Dr.Eng. from Kyoto University under the supervision of Prof. Kohei Tamao in 1997. Before receiving his Dr. degree, in 1993, he was appointed as an assistant professor at Institute for Chemical Research, Kyoto University. In 2003, he moved to Nagoya University as an associate professor, and in 2005, he promoted to a full professor at the same place. Meanwhile, he spent a year (2000–2001) as a visiting scientist at Massachusetts Institute of Technology. His current research is broadly focused on the development of new functional π-conjugated materials directed toward organic electronics and bioimaging applications.

Abstract

Fluorophores with intramolecular charge-transfer (ICT) character in the excited state exhibit significant solvatochromism of their fluorescence. Here, we report an example for such compounds, a benzophosphole *P*-oxide bearing an electron-donating *p*-(diphenylamino)phenyl group at the 3-position. While this compound shows only subtle dependence of the absorption maximum on the solvent polarity ($\lambda_{max} = 383$–392 nm), its emission maximum is significantly red-shifted upon increasing the solvent polarity (cyclohexane: $\lambda_{em} = 457$ nm; DMF: $\lambda_{em} = 598$ nm). Most notably, the fluorescence quantum yields gradually increase with increased Stokes shifts, ultimately reaching $\Phi_F = 0.28$ in DMF. This trend is fundamentally different from that observed for the corresponding 2-(diphenylamino)phenyl-substituted benzophosphole congener, for which applications as a fluorescent bioimaging probe were previously demonstrated. In this study, the origins of this striking difference are examined by a combined experimental and theoretical approach. Our results suggest that the observed difference arises from a significant contribution of quinoidal resonance forms in the ICT excited state, which suppresses nonradiative decay and hence increases the quantum yield in polar solvents.

Intramolecular charge-transfer (ICT) transitions generate highly polarized excited states, which are sensitive to the polarity of the reaction medium.[1] Accordingly, fluorophores that are characterized by ICT in the excited state show significant solvatochromism of their fluorescence. Such fluorescent molecules have great potential as environment-sensitive fluorescent bioimaging probes,[2] which can visualize polarity changes associated with cellular events. This class of molecules usually consists of electron-donating and electron-accepting moieties, and several fascinating fluorescent probes, such as prodan,[3] 1,8-ANS,[4] Dapoxyl,[5] and Nile red,[6] have been developed.

One crucial requirement for this class of fluorophores is the ability to maintain intense emissions even in polar solvents. As the ICT excited state is usually associated with a large structural relaxation, and tends to undergo an accelerated nonradiative decay, a special mechanism or suitable skeleton is necessary in order to simultaneously generate a large Stokes shift and an intense emission.[3,7] In this context, we have recently reported the outstanding behavior of a benzophosphole *P*-oxide skeleton to act as an effective electron-accepting unit for donor–acceptor-type fluorophores (Figure 1).[8,9] Compound **1**, bearing an electron-donating *p*-(*N*,*N*-diphenylamino)phenyl group (hereafter denoted simply aminophenyl group) at the 2-position, maintains high fluorescence quantum yields even in polar ($\Phi_F = 0.64$ in DMSO) or protic ($\Phi_F = 0.58$ in ethanol) solvents, while significant Stokes shifts were maintained in these solvents. However, this compound still obeyed the general trend of gradually decreasing fluorescence quantum yields as a function of increasing solvent polarity.

In sharp contrast to the behavior of **1**, we have now discovered that an analogous benzophosphole *P*-oxide **2a**, bearing the aminophenyl group at the 3-position, exhibited diametrally opposed fluorescence properties, i.e. a gradual increase in

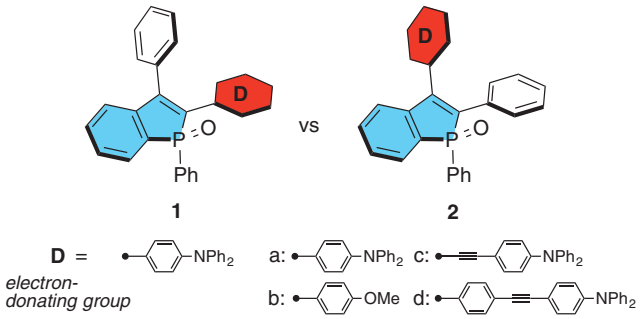

Figure 1. Chemical structures of benzophosphole *P*-oxides **1** and **2**.

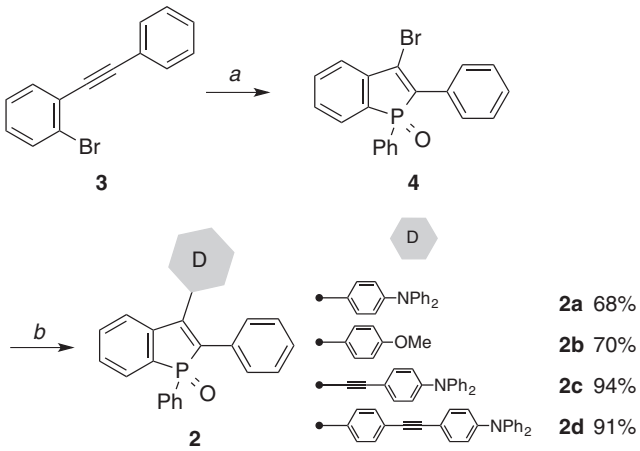

Scheme 1. Reagents and conditions: *a*, 1) *t*-BuLi, THF, −78 °C; 2) $PhP(NEt_2)Cl$, −78 °C; 3) PBr_3, rt, 4) H_2O_2 aq.; *b*, for **2a** and **2b**: $ArB(OH)_2$ (**2a**: Ar = 4-(*N*,*N*-diphenylamino)phenyl; **2b**: Ar = 4-methoxyphenyl), $[Pd_2(dba)_3]\cdot CHCl_3$ (2.5 mol %), S-Phos (5 mol %), K_3PO_4, toluene/H_2O, 80 °C; for **2c**: *N*,*N*-diphenyl-4-ethynylaniline, $[Pd(PPh_3)_4]$ (1 mol %), CuI (2 mol %), Et_3N, THF, 80 °C; for **2d**: 4-[4-(*N*,*N*-diphenylamino)phenylethynyl]phenylboronic acid, $[Pd(PPh_3)_4]$ (10 mol %), K_3PO_4, toluene/H_2O, 80 °C.

fluorescence quantum yields with increasing solvent polarity. In the present article, we would like to disclose the details of this phenomenon together with an examination of its origins, based on comparative studies with analogues **2b**–**2d** and quantum chemical calculations. A key factor in suppressing the nonradiative decay in this type of molecule is the more pronounced quinoidal contribution to the character of its excited state.

Results and Discussion

A series of benzophosphole oxides with electron-donating aryl groups at the 3-position was synthesized following a previously reported method (Scheme 1).[10,11] As a key precursor, 3-bromo-2-phenylbenzophosphole oxide **4** was obtained in a one-pot synthesis from *o*-bromo-substituted diphenylacetylene **3**. Compound **3** was treated with *t*-BuLi followed by addition of an aminochlorophosphine to produce the corresponding aminophosphanyl-substituted intermediate. Without isolation, treatment with PBr_3 promoted an intramolecular *trans*-halophosphanylation by bromination of the amino group

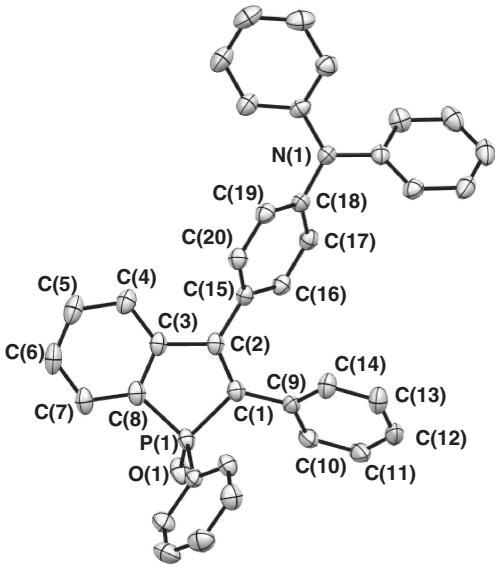

Figure 2. ORTEP drawing of **2a**. Thermal ellipsoids are drawn at 50% probability. Hydrogen atoms are omitted for clarity. Selected bond lengths (Å), bond angles (deg), and torsion angles (deg): N(1)–C(18) = 1.415(2), P(1)–C(1) = 1.8067(18), P(1)–C(8) = 1.8017(19), C(1)–C(2) = 1.354(2), C(1)–C(9) = 1.483(2), C(2)–C(3) = 1.494(2), C(2)–C(15) = 1.479(2), C(3)–C(8) = 1.401(3), C(9)–C(10) = 1.391(3), C(10)–C(11) = 1.395(3), C(11)–C(12) = 1.374(3), C(15)–C(16) = 1.399(2), C(16)–C(17) = 1.380(3), C(17)–C(18) = 1.393(3), P(1)–C(1)–C(2) = 110.64(13), C(1)–P(1)–C(8) = 92.38(8), C(1)–C(2)–C(3) = 114.25(15), C(2)–C(3)–C(8) = 113.27(15), C(3)–C(8)–P(1) = 109.42(13), C(2)–C(1)–C(9)–C(14) = 46.7(3), C(3)–C(2)–C(15)–C(20) = 48.4(2).

on phosphorus. Further oxidation with hydrogen peroxide afforded the 3-bromo-substituted benzophosphole *P*-oxide **4**. An advantage of this method in comparison with other benzophosphole syntheses[12] is that it allows the facile introduction of various aryl groups at the 3-position of the benzophosphole skeleton via palladium-catalyzed cross-coupling reactions. Indeed, Suzuki–Miyaura and Sonogashira coupling protocols furnished target compounds **2a**–**2d** in good yields (68–94%).

The molecular structure of **2a** was obtained from X-ray crystallographic analysis, and is shown in Figure 2; it revealed a propeller-like arrangement of the peripheral aryl groups, whereby the dihedral angles between the phosphole ring and the benzene rings at the 2- and 3-positions are 46.7 and 48.4°, respectively. Due to the fused benzene ring, the phosphole ring is slightly distorted, exhibiting C(1)–C(2) and C(3)–C(8) bond lengths of 1.354(2) and 1.401(3) Å, respectively. The phenyl groups at the 2- and 3-position did not exhibit any significant bond alternations.

Benzophosphole *P*-oxide **2a**, bearing an electron-donating aminophenyl group at the 3-position, exhibited intriguing photophysical properties (Figure 3 and Table 1). Its absorption spectrum in DMF showed an absorption maximum at 384 nm with a moderate molar extinction coefficient ($\varepsilon = 7530$ $M^{-1}\,cm^{-1}$). In the same solvent, the fluorescence spectrum showed a reddish-orange emission ($\lambda_{max} = 598$ nm), and

despite the considerable Stokes shift (9320 cm^{-1}), the fluorescence quantum yield was quite substantial ($\Phi_F = 0.28$). Given the low fluorescence quantum yield of 1,2,3-triphenylbenzo[*b*]-phosphole *P*-oxide in THF ($\Phi_F = 0.01$), this contrast is quite remarkable.[13]

Even though the photophysical properties of **2a** are comparable to those of the 2-aminophenyl-substituted congener **1** ($\lambda_{abs} = 409$ nm, $\lambda_{em} = 598$ nm, $\Phi_F = 0.71$ in DMF), the solvent dependence of the fluorescence of these two compounds is intrinsically different. Both compounds showed significant bathochromic shifts with increasing solvent polarity. The corresponding Lippert–Mataga plots[1] for both compounds in various solvents were highly linear (**1**: $R^2 = 0.93$, **2a**: $R^2 = 0.87$; Figure S6), suggesting that specific solvent effects, such as hydrogen bonding, do not affect the photophysical properties. Similar to other donor–acceptor-type fluorophores, **1** showed a significant decrease in Φ_F with increasing bathochromic shifts. In contrast to that, **2a** exhibited the opposite behavior (Figure 4): in cyclohexane, a small Stokes shift of 4200 cm^{-1} and a Φ_F of merely 0.05 were observed, whereby the value of the latter increased with increasing solvent polarity.

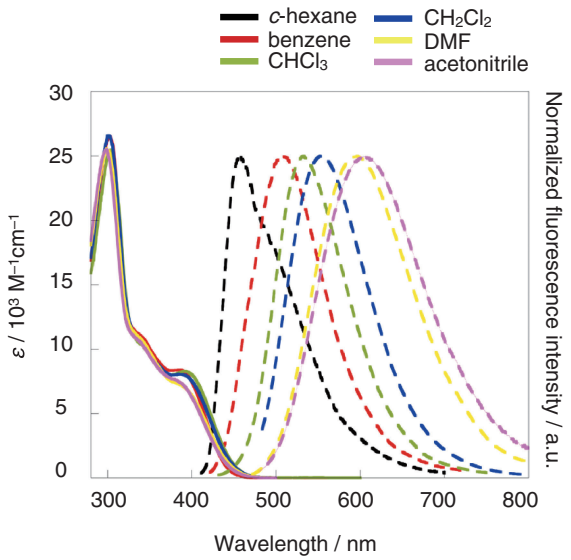

Figure 3. Absorption (solid line) and fluorescence spectra (broken line) of **2a** in various solvents.

To investigate the effect of the nature of the aryl group at the 3-position, we compared the properties of **2a** with **2b**, which contains a weaker electron-donating anisyl group at the same position (Table 1). Notably, **2b** did not exhibit any solvent dependence; neither for the fluorescence maximum wave-

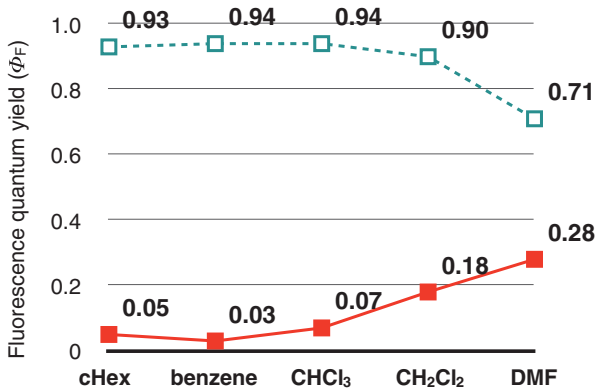

Figure 4. Fluorescence quantum yield of **1** (dashed line) and **2a** (solid line) in various solvents (cHex: cyclohexane, DMF: *N*,*N*-dimethylformamide).

Table 1. Photophysical properties of benzophosphole *P*-oxides **2a**–**2d** in various solvents

Cmpd	Solvents	λ_{abs} /nm[a)]	ε /M^{-1} cm^{-1}	λ_{em} /nm[a)]	Φ_F[b)]	Stokes shift /cm^{-1}	τ /ns	k_r /10^8 s^{-1}	k_{nr} /10^8 s^{-1}
2a	cyclohexane	383	—[c)]	457	0.050	4200	0.28	1.7	33
	benzene	392	8190	509	0.025	5860	0.34	0.73	29
	$CHCl_3$	390	8280	533	0.072	6880	0.73	0.98	13
	CH_2Cl_2	390	8010	552	0.18	7530	2.0	0.90	4.1
	DMF	384	7530	598	0.28	9320	4.9	0.56	1.5
	acetonitrile	384	7490	606	0.27	9540	4.8	0.50	1.5
2b	cyclohexane	348	—[c)]	444	—[d)]	6200	—[d)]	—[d)]	—[d)]
	benzene	352	5800	449	—[d)]	6200	—[d)]	—[d)]	—[d)]
	$CHCl_3$	353	7120	450	0.009	6100	—[d)]	—[d)]	—[d)]
	CH_2Cl_2	351	7310	446	0.010	6100	—[d)]	—[d)]	—[d)]
	DMF	350	12400	447	0.009	6200	—[d)]	—[d)]	—[d)]
2c	cyclohexane	419	23800	461	0.62	2200	2.4	2.6	1.6
	benzene	428	22300	503	0.62	3500	2.6	2.3	1.5
	$CHCl_3$	437	24500	548	0.86	4640	4.4	1.9	0.33
	CH_2Cl_2	433	24300	584	0.68	5970	5.7	1.2	0.57
	DMF	435	24500	648	0.13	7560	1.7	0.81	5.3
2d	cyclohexane	356	33100	455	0.46	6100	1.7	2.6	3.1
	benzene	358	30000	480	0.53	7100	1.9	2.8	2.5
	$CHCl_3$	353	31300	547	0.79	10000	4.3	1.9	0.48
	CH_2Cl_2	353	32100	608	0.70	11900	6.3	1.1	0.48
	DMF	351	32400	685	0.027	13900	0.27	1.0	36

a) Only the longest absorption or emission maximum wavelengths are shown. b) Absolute quantum yield determined by a calibrated integrating sphere system. c) Not determined due to very low solubility. d) Not determined due to insufficient fluorescence.

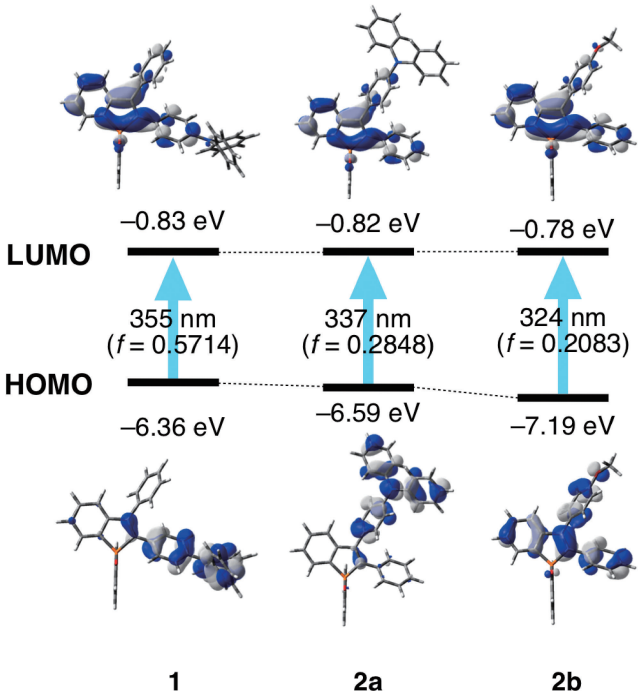

Figure 5. Kohn–Sham molecular orbitals, excitation energies, and oscillator strengths calculated at the TD-CAM-B3LYP/6-311G(d) level for the optimized structures of **1**, **2a**, and **2b** in their electronic singlet ground state (S_0). Only the electronic transitions with the highest contribution are shown.

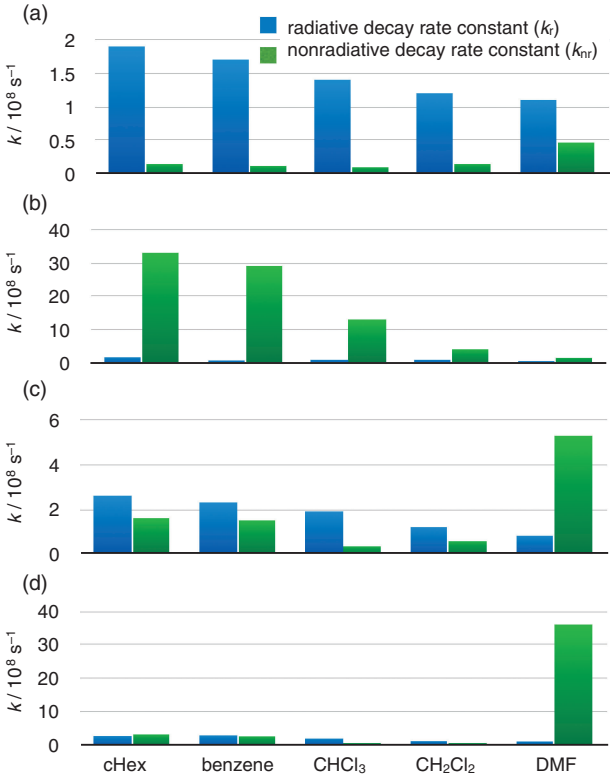

Figure 6. Rate constants for radiative (blue) and nonradiative (green) decay of (a) **1**, (b) **2a**, (c) **2c**, and (d) **2d** in various solvents.

length, nor for the fluorescence quantum yield. Irrespective of the solvent polarity, **2b** showed weak fluorescence with a maximum around 450 nm and low Φ_F values. This result indicates that the strongly electron-donating amino group in **2a** plays a pivotal role in the unusual solvent dependence of the fluorescence quantum yield. The low Φ_F observed for **2b** may be partly due to the intramolecular rotation or vibration of the 2,3-aryl groups in solution, similar to tetraarylsiloles[14] and -phospholes.[15]

Density functional theory (DFT) calculations at the CAM-B3LYP/6-311G(d) level highlighted a clear difference between **2a** and **2b** in terms of the nature of the electronic transitions (Figure 5). The optimized structure of **2a** was consistent with that of X-ray crystal structure. The $S_0 \rightarrow S_1$ transition in **2b** is mainly attributable to the π–π^* transition of the 2-phenyl-substituted benzophosphole moiety. In sharp contrast, the $S_0 \rightarrow S_1$ transition in **2a** consists predominantly of the intramolecular charge transfer (ICT) from the HOMO localized on the electron-donating 3-(aminophenyl) group to the LUMO localized on the benzophosphole *P*-oxide skeleton. Therefore, the ICT character of S_1 is the key to induce the observed solvent dependence of the fluorescence in **2a**.

The DFT calculations also revealed an interesting similarity in the electronic structure between **1** and **2a** (Figure 5). The HOMO of benzophosphole oxide **1**, which contains the donor substituent at the 2-position, is localized primarily around the aminophenyl moiety, whereas the LUMO is localized mainly on the benzophosphole *P*-oxide moiety. Even though both energy levels are comparable to those of 3-substituted **2a**, these two compounds exhibit a contrasting solvent dependence of the fluorescence as described above. To determine the origin of this discrepancy, we further studied the dynamics of **1** and **2a** in the excited state, starting by fluorescence lifetime (τ) measurements in various solvents. Based on these, and the previously established Φ_F values, radiative (k_r) and nonradiative (k_{nr}) decay rate constants were calculated. Figure 6 clearly shows that for **1**, the decrease in Φ_F with increasing solvent polarity is due to a combination of decreased k_r and increased k_{nr} values, while the Φ_F values of **2a** are mainly governed by the k_{nr} values. Upon increasing the polarity from nonpolar cyclohexane to polar DMF, the k_{nr} values for **2a** decrease by ca. 90%.

The significant decline of k_{nr} values for **2a** in polar solvents should be related to the structure of its excited state.[16,17] Therefore, we calculated the optimized structures of **2a** and **1** in the first excited singlet S_1 state at the TD-CAM-B3LYP/6-31G(d) level of theory (Figures 7 and S8). While the phenyl groups at the 2- and 3-positions in the S_0 state of **2a** are oriented in a twisted fashion relative to the benzophosphole plane (dihedral angles: 41.3°/57.9°), their orientation becomes more coplanar in S_1 (22.3°/41.0°). Simultaneously, the bond alternation mode also changes significantly from S_0 to S_1. Not only the aminophenyl group at the 3-position, but also the phenyl group at the 2-position adopt a more quinoidal structure in S_1. From S_0 to S_1, the lengths of the bonds connecting the phosphole ring and the phenyl groups at the 2- and 3-position are shortened by 0.047 and 0.043 Å, respectively. This change should reflect the ICT character of the $S_0 \rightarrow S_1$ transition.

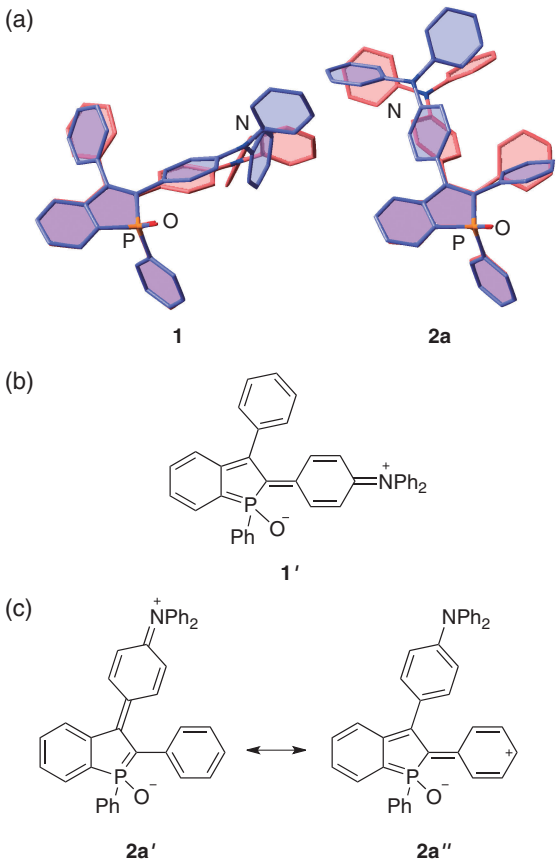

Figure 7. Structural changes in **1** and **2a** between ground (S_0) and first excited singlet state (S_1) geometries: (a) Superimposed drawing of the structures for S_0 (blue) and S_1 (red) for **1** and **2a** (top panel), as well as dominant resonance forms in S_1 for (b) **1** and (c) **2a** (bottom panel).

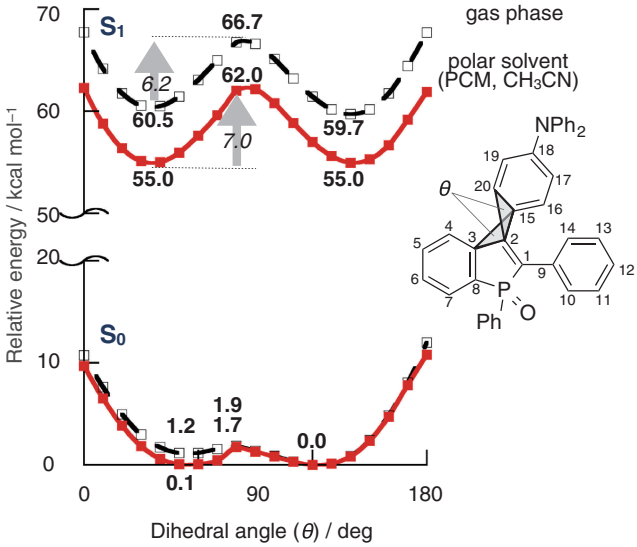

Figure 8. Energy diagrams for S_0 (bottom) and S_1 (top) of **2a** in the gas phase (dashed line) and in solution (acetonitrile; solid line) as a function of the dihedral angle θ (C3–C2–C15–C20). Geometry optimizations and energies of S_0 and S_1 were calculated at the CAM-B3LYP/BS (BS N: 6-31+G(d); BS C, H, O, P: 6-31G(d)) and TD-CAM-B3LYP/BS levels, respectively. The solvent effect was calculated using the polarizable convent model (PCM).

Indeed, a natural population analysis (NPA)[18] of the S_1 state at the (TD)-CAM-B3LYP/6-311G(d) level suggests that the electronic charge is transferred from both phenyl groups at the 2- and 3-position to the phosphole skeleton (Figure S9). Upon changing from S_0 to S_1, Wiberg bond indices (WBI) increase from 1.05 to 1.23 and from 1.01 to 1.16 for the bonds connecting the phosphole with the phenyl groups at the 2- and 3-positions, respectively (Figure S10). Taking these features into account, the structure of **2a** in S_1 may be best described by resonance structures **2a′** and **2a″** (Figure 7c). This structural change contrasts to that in 2-substituted congener **1**, which only shows a quinoidal contribution from the aminophenyl group at the 2-position, like the canonical structure of **1′** (Figures S8–S10). The greater contribution of the quinoidal character in **2a** might be responsible for its smaller k_{nr} value compared to that of **1**.

We assumed that for compound **2a**, the quinoidal character in S_1 is enhanced in polar solvents, which should result in a suppression of the intramolecular rotation/vibration of the phenyl groups at the 2- and 3-position, thus facilitating the decrease of the k_{nr} value. In order to test this hypothesis, we calculated gas phase rotational barriers of the 3-phenyl group in **2a** for the ground and excited state (Figure 8). For that purpose, we used separate relaxed potential energy scans for the S_0 and S_1 surfaces. Relative energies were calculated by changing the dihedral angle θ (C3–C2–C15–C20) in increments of 10°. Subsequently, the molecular geometries for the S_0 and S_1 states were optimized for each dihedral angle using the CAM-B3LYP functional and the 6-31+G(d) or 6-31G(d) basis sets for the N and the C, H, O, and P atoms, respectively. Even though energy barriers were found close to 90° for both the ground and excited states, the activation energy in the excited state is higher than that in the ground state. To investigate the solvent effect, energy barriers were calculated by using the polarizable convent model (PCM), employing acetonitrile as a representative polar solvent.[19] Compared to the gas phase, the relative energies of S_1 in the polar solvent are stabilized irrespective of the dihedral angle. However, while the energy barrier for S_1 in the gas phase is about 6.2 kcal mol^{-1}, it is increased to 7.0 kcal mol^{-1} in acetonitrile. The intramolecular bond rotation/vibration of the phenyl group in 3-position is therefore suppressed to a greater extent in polar solvents relative to nonpolar solvents. Accordingly, this result is consistent with the experimental observation of decreased k_{nr} values in polar solvents.

Furthermore, we found that a direct attachment of the electron-donating group to the benzophosphole skeleton is crucial to induce increased Φ_F with increased solvent polarity. This is demonstrated by comparing the fluorescence properties of **2c** and **2d**, which connect the aminophenyl group with either an ethynyl or phenylethynyl spacer. Whereas both compounds showed increased Φ_F values upon increasing the solvent polarity from cyclohexane to chloroform, the Φ_F values significantly decreased in more polar solvents such as DMF (Table 1). The k_r and k_{nr} values for **2c** and **2d** were also determined, whereby the k_{nr} values were found to decrease from cyclohexane to chloroform. In more polar solvents, however, the k_{nr} values

were found to increase (Figures 6c and 6d), which is in stark contrast to the trend observed for **2a**. This increase of the k_{nr} values for **2c** and **2d** in polar solvents is in good explained by the energy gap law for nonradiative decay associated with the significant red shift of fluorescence.[20]

Conclusion

We discovered an unusual solvent dependence of the fluorescence properties in benzophosphole *P*-oxide **2a**, which bears an electron-donating aminophenyl group at the 3-position. In contrast to 2-(aminophenyl)-substituted congener **1**, **2a** exhibited increased Φ_F with increasing solvent polarity, while simultaneously showing a large Stokes shift. In general, the contribution of a 3-aryl group to the π-conjugation in heterole or benzoheterole rings is not considered to be significant. However, the present results demonstrate that the substituent at the 3-position influences the excited state through an intramolecular charge-transfer transition. The observed unusual fluorescence properties of **2a** result most likely from a substantial contribution of a quinoidal resonance structure to the first excited singlet electronic state (S_1). These results thus provide important new guidelines for the design of unprecedented fluorescent molecules.

Experimental

General. Melting points (mp) or decomposition temperatures were determined with a Stanford Research Systems OptiMelt MPA100 instrument. ^{1}H, ^{13}C{^{1}H}, and ^{31}P{^{1}H} spectra were recorded with a JEOL AL-400 spectrometer (400 MHz for ^{1}H, 100 MHz for ^{13}C, 162 MHz for ^{31}P) in CD_2Cl_2. The chemical shifts in ^{1}H and ^{13}C NMR spectra are reported in δ ppm using the residual proton of the solvents (5.30 ppm) or the solvent signals of CD_2Cl_2 (53.84 ppm) as an internal standard, respectively. The chemical shifts in ^{31}P NMR spectra are reported using H_3PO_4 (0.00 ppm) as an external standard. Mass spectra were measured with a Bruker micrOTOF Focus spectrometer with the APCI ionization method. Thin layer chromatography (TLC) was performed on plates coated with 0.25 mm thick silica gel 60F_{254} (Merck). Column chromatography was performed using PSQ100B (Fuji Silysia Chemicals). Recycling preparative gel permeation chromatography (GPC) was performed using an LC-918 (Japan Analytical Industry) equipped with polystyrene gel columns (JAIGEL 1H and 2H, Japan Analytical Industry) and $CHCl_3$ as the eluent. All reactions were carried out under an argon atmosphere. 3-Bromo-1,2-diphenylbenzo[*b*]phosphole *P*-oxide **4**[11] and 4-[4-(*N*,*N*-diphenylamino)phenylethynyl]phenylboronic acid[21] were prepared according to the literature methods.

1,2-Diphenyl-3-[4-(*N*,*N*-diphenylamino)phenyl]benzo[*b*]-phosphole *P*-Oxide (2a). To a solution of **4** (0.192 g, 0.503 mmol) in a mixed solvent of toluene (10 mL) and water (2.5 mL) was added 4-(*N*,*N*-diphenylamino)phenylboronic acid (0.160 g, 0.553 mmol), $[Pd_2(dba)_3]\cdot CHCl_3$ (13.9 mg, 0.0134 mmol), S-Phos (10.1 mg, 0.0246 mmol) and K_3PO_4 (0.161 g, 0.758 mmol). The mixture was heated at 80 °C with stirring for 44 h and then extracted with chloroform. The combined organic layer was washed with brine, dried over anhydrous Na_2SO_4, and filtered. After removing solvents under reduced pressure, the yellow solid was subjected to silica gel column chromatography ($CHCl_3$/AcOEt 8:1, $R_f = 0.30$) to afford 0.186 g (0.340 mmol, 68% yield) of **2a** as yellow solids. Mp: 206.7–207.0 °C (decomp.). ^{1}H NMR (400 MHz, CD_2Cl_2): δ 7.74–7.63 (m, 3H), 7.54–7.46 (m, 2H), 7.40–7.31 (m, 4H), 7.30–7.26 (m, 6H), 7.20–7.11 (m, 9H), 7.08–7.04 (m, 4H). ^{13}C{^{1}H} NMR (100 MHz, CD_2Cl_2): δ 150.4 (d, $J_{CP} = 21.4$ Hz, C), 148.9 (s, C), 147.8 (s, C), 144.2 (d, $J_{CP} = 26.4$ Hz, C), 134.2 (d, $J_{CP} = 91.4$ Hz, C), 133.7 (d, $J_{CP} = 5.0$ Hz, C), 133.3 (d, $J_{CP} = 2.0$ Hz, CH), 133.0 (d, $J_{CP} = 105$ Hz, C), 132.5 (s, C), 131.4 (d, $J_{CP} = 9.9$ Hz, CH), 130.8 (d, $J_{CP} = 99.0$ Hz, C), 130.6 (s, CH), 129.8 (s, CH), 129.5 (d, $J_{CP} = 5.7$ Hz, CH), 129.5 (d, $J_{CP} = 9.9$ Hz, CH), 129.3 (d, $J_{CP} = 12.4$ Hz, CH), 129.1 (d, $J_{CP} = 9.1$ Hz, CH), 128.6 (s, CH), 128.2 (s, CH), 127.7 (d, $J_{CP} = 14.8$ Hz, C), 125.4 (s, C), 124.6 (d, $J_{CP} = 10.7$ Hz, C), 124.0 (s, C), 123.1 (s, C). ^{31}P{^{1}H} NMR (162 MHz, CD_2Cl_2): δ 38.1. HRMS (APCI): m/z calcd. for $C_{38}H_{28}NOP$: 545.1903 ($[M]^+$); found. 545.1921.

1,2-Diphenyl-3-(4-methoxyphenyl)benzo[*b*]phosphole *P*-Oxide (2b). This compound was prepared essentially in the same manner as described for **2a** using **4** (0.199 g, 0.523 mmol), 4-methoxyphenylboronic acid (83.1 mg, 0.547 mmol), $[Pd_2(dba)_3]\cdot CHCl_3$ (12.4 mg, 0.0120 mmol), S-Phos (10.5 mg, 0.0256 mmol), and K_3PO_4 (0.162 g, 0.763 mmol). The mixture was purified by silica gel column chromatography ($CHCl_3$/AcOEt 8:1, $R_f = 0.35$), and further purified by GPC to afford 0.149 g (0.366 mmol, 70% yield) of **2b** as colorless solids. Mp: 189.7–189.9 °C (decomp.). ^{1}H NMR (400 MHz, CD_2Cl_2): δ 7.72 (dd, $J = 12.0$, 8.0 Hz, 2H), 7.63 (t, $J = 8.4$ Hz, 1H), 7.48 (t, $J = 7.2$ Hz, 2H), 7.41–7.36 (m, 3H), 7.29–7.26 (m, 3H), 7.23–7.21 (m, 2H), 7.23–7.11 (m, 3H), 6.95 (d, $J = 8.0$ Hz, 2H), 3.83 (s, 3H). ^{13}C{^{1}H} NMR (100 MHz, CD_2Cl_2): δ 160.5 (s, C), 150.3 (d, $J_{CP} = 21.4$ Hz, C), 144.3 (d, $J_{CP} = 26.4$ Hz, C), 134.3 (d, $J_{CP} = 95.5$ Hz, C), 133.7 (d, $J_{CP} = 9.9$ Hz, C), 133.2 (s, CH), 133.0 (d, $J_{CP} = 104$ Hz, C), 132.5 (d, $J_{CP} = 2.4$ Hz, CH), 131.4 (d, $J_{CP} = 10.7$ Hz, CH), 131.0 (s, CH), 131.0 (d, $J_{CP} = 98.0$ Hz, C), 129.5 (d, $J_{CP} = 9.9$ Hz, CH), 129.5 (d, $J_{CP} = 4.9$ Hz, CH), 129.3 (d, $J_{CP} = 12.3$ Hz, CH), 129.1 (d, $J_{CP} = 9.0$ Hz, CH), 128.7 (s, CH), 128.1 (s, CH), 126.6 (d, $J_{CP} = 15.7$ Hz, C), 124.5 (d, $J_{CP} = 11.5$ Hz, CH), 114.8 (s, CH), 55.7 (s, CH_3). ^{31}P{^{1}H} NMR (162 MHz, CD_2Cl_2): δ 38.0. HRMS (APCI): m/z calcd. for $C_{27}H_{21}O_2P$: 409.1274 ($[M]^+$); found. 408.1289.

1,2-Diphenyl-3-{[4-(*N*,*N*-diphenylamino)phenyl]ethynyl}-benzo[*b*]phosphole *P*-Oxide (2c). To a solution of **4** (0.376 g, 0.987 mmol), $[Pd(PPh_3)_4]$ (13.1 mg, 0.0113 mmol) and CuI (3.8 mg, 0.020 mmol) in triethylamine (5 mL) was added *N*,*N*-diphenyl-4-ethynylaniline in THF (5 mL) dropwise over 5 min. The mixture was heated at 80 °C with stirring for 18 h, and then water was added. The mixture was extracted with chloroform. The combined organic layer was washed with brine, dried over anhydrous Na_2SO_4, and filtered. After removing solvents under reduced pressure, the red solid was subjected to silica gel column chromatography ($CHCl_3$/AcOEt 8:1, $R_f = 0.26$). The solid obtained was recrystallized from AcOEt to afford 0.527 g (0.924 mmol, 94% yield) of **2c** as yellow crystals. Mp: 117.8–118.2 °C (decomp.). ^{1}H NMR (400 MHz, CD_2Cl_2): δ 8.13 (d, $J = 8.4$ Hz, 2H), 7.85 (dd, $J = 7.6$, 3.2 Hz, 1H), 7.71–7.57 (m, 4H), 7.45–7.29 (m, 13H), 7.15–7.10 (m, 6H), 7.00 (d, $J = 8.8$ Hz, 2H). ^{13}C{^{1}H} NMR (100 MHz, CD_2Cl_2): δ 149.9 (s, C), 147.2 (s, C), 142.3 (d, $J_{CP} = 24.7$ Hz, C), 138.0 (d, $J_{CP} = 97.9$

Hz, C), 133.8 (d, $J_{CP} = 9.0$ Hz, C), 133.7 (s, CH), 133.6 (d, $J_{CP} = 9.1$ Hz, C), 133.6 (s, C), 132.6 (d, $J_{CP} = 2.5$ Hz, CH), 131.8 (d, $J_{CP} = 105$ Hz, C), 131.3 (d, $J_{CP} = 10.7$ Hz, CH), 131.2 (d, $J_{CP} = 100$ Hz, C), 130.0 (s, CH), 129.9 (d, $J_{CP} = 10.7$ Hz, CH), 129.3 (d, $J_{CP} = 17.3$ Hz, CH), 129.3 (d, $J_{CP} = 12.4$ Hz, CH), 128.9 (s, CH), 128.7 (s, CH), 128.6 (d, $J_{CP} = 6.5$ Hz, CH), 126.1 (s, CH), 124.8 (s, CH), 124.1 (d, $J_{CP} = 10.7$ Hz, CH), 121.6 (s, CH), 114.2 (s, C), 104.4 (s, C), 84.2 (d, $J_{CP} = 23.1$ Hz, C). $^{31}P\{^1H\}$ NMR (162 MHz, CD_2Cl_2): δ 38.4. HRMS (APCI): m/z calcd. for $C_{40}H_{29}NOP$: 570.1981 ($[M + H]^+$); found. 570.1968.

1,2-Diphenyl-3-{4-[4-(*N*,*N*-diphenylamino)phenylethynyl]phenyl}benzo[*b*]phosphole *P*-Oxide (2d). This compound was prepared essentially in the same manner as described for **2a** using **4** (0.153 g, 0.400 mmol) in toluene (4 mL) and water (1 mL), 4-[4-(*N*,*N*-diphenylamino)phenylethynyl]phenylboronic acid (0.185 g, 0.476 mmol), $[Pd(PPh_3)_4]$ (48.3 mg, 41.8 μmol), and K_3PO_4 (0.128 g, 0.601 mmol). The mixture was purified by silica gel column chromatography ($CHCl_3$/AcOEt 10:1, $R_f = 0.28$). The obtained solid was further purified by washing with small amount of CH_2Cl_2 and hexane to give 0.236 g of **2d** (0.365 mmol, 91% yield) as yellow solids. Mp: 134.5–135.4 °C (decomp.). ^1H NMR (400 MHz, CD_2Cl_2): δ 7.72 (ddd, $J = 12.0$, 8.4, 1.2 Hz, 2H), 7.65 (d, $J = 8.4$ Hz, 1H), 7.56 (d, $J = 8.0$ Hz, 2H), 7.52–7.47 (m, 2H), 7.42–7.21 (m, 14H), 7.13–7.05 (m, 9H), 6.97 (d, $J = 8.8$ Hz, 2H). $^{13}C\{^1H\}$ NMR (100 MHz, CD_2Cl_2): δ 149.8 (d, $J_{CP} = 21.4$ Hz, C), 148.8 (s, C), 147.6 (s, C), 143.8 (d, $J_{CP} = 26.4$ Hz, C), 135.4 (d, $J_{CP} = 93.8$ Hz, C), 134.3 (d, $J_{CP} = 14.8$ Hz, C), 133.4 (s, CH), 133.3 (d, $J_{CP} = 13.1$ Hz, C), 133.0 (s, CH), 132.8 (d, $J_{CP} = 110$ Hz, C), 132.6 (d, $J_{CP} = 2.5$ Hz, CH), 132.3 (s, CH), 131.4 (d, $J_{CP} = 10.7$ Hz, CH), 130.7 (d, $J_{CP} = 99.6$ Hz, C), 129.9 (s, CH), 129.8 (s, CH), 129.7 (d, $J_{CP} = 13.2$ Hz, CH), 129.5 (d, $J_{CP} = 5.8$ Hz, CH), 129.3 (d, $J_{CP} = 11.5$ Hz, CH), 129.3 (d, $J_{CP} = 9.1$ Hz, CH), 128.8 (s, CH), 128.4 (s, CH), 125.9 (s, CH), 124.5 (s, C), 124.5 (d, $J_{CP} = 10.7$ Hz, CH), 124.2 (s, CH), 122.3 (s, CH), 115.9 (s, C), 91.4 (s, C), 88.5 (s, C). $^{31}P\{^1H\}$ NMR (162 MHz, CD_2Cl_2): δ 38.0. HRMS (APCI): m/z calcd. for $C_{46}H_{33}NOP$: 646.2294 ($[M + H]^+$); found. 646.2274.

Photophysical Measurements. UV–vis absorption spectra were measured with a Shimadzu UV-3150 spectrometer with a resolution of 0.2 nm using ca. 10^{-5} M sample solutions in spectral grade solvents in a 1 cm square quartz cuvette. Emission spectra were measured with a Hitachi F-4500 spectrometer with a resolution of 1 nm. Absolute fluorescence quantum yields were determined with a Hamamatsu photonics PMA-11 calibrated integrating sphere system. Time-resolved fluorescence spectra were measured with a Hamamatsu Picosecond Fluorescence Measurement System C4780 equipped with a picosecond light pulser PLP-10 (excitation wavelength 377 nm with a repetition rate of 10 Hz). All the decay profiles were fitted reasonably well using a single exponential function.

X-ray Data Collection of 2a. Block-shaped yellow single crystals were grown by recrystallization from MeOH/CH_2Cl_2. Intensity data ware collected at 123 K on a Rigaku Single Crystal CCD X-ray diffractometer (Saturn 70 with MicroMax-007) with Mo Kα radiation ($\lambda = 0.71075$ Å) and graphite monochromator. A total of 10942 reflections were measured with the maximum 2θ angle of 50.0°, of which 4771 were independent reflections ($R_{int} = 0.0214$). The structure was solved by direct methods (SHELXS-97 or SHELXS-2013)[22,23] and refined by the full-matrix least-squares on F^2 (SHELXL-2013). All non-hydrogen atoms were refined anisotropically and all hydrogen atoms were placed using AFIX instructions. The crystal data are as follows: $C_{38}H_{28}NOP$; FW = 545.58, crystal size $0.16 \times 0.15 \times 0.12$ mm^3, triclinic, $P\bar{1}$ (#2), $a = 10.179(4)$ Å, $b = 10.284(4)$ Å, $c = 14.338(6)$ Å, $\alpha = 109.581(6)°$, $\beta = 91.482(4)°$, $\gamma = 94.596(4)°$, $V = 1407.3(10)$ Å^3, $Z = 2$, $D_c = 1.287$ g cm^{-3}, $\mu = 0.130$ mm^{-1}, $R_1 = 0.0399$ ($I > 2\sigma(I)$), $wR_2 = 0.1042$ (all data), GOF = 1.039. CCDC 1050579.

Computational Method. Geometry optimizations for electronic singlet ground S_0 and first excited S_1 states of **1** and **2a** were performed using the CAM-B3LYP and TD-CAM-B3LYP theory, respectively, with the 6-31G(d) basis set, as implemented in the Gaussian 09 program.[24] All stationary points were optimized without any symmetry constraint and stationary points on the electronic ground states were characterized by normal coordinate analysis at the same level of theory (the number of imaginary frequencies, NIMAG, was 0 for minima). TD-DFT vertical excitation calculations were also performed using the TD-CAM-B3LYP theory with the 6-31G(d) basis set. The solvent effect was included using the polarizable continuum model (PCM). Natural population analysis (NPA) for the ground and excited states were carried out using the Gaussian 09 program based on the optimized structures of **1** and **2** at the (TD-)CAM-B3LYP/6-311G(d) level of theory.

This work was partly supported by JST, CREST (S.Y. and S.I.) and a Grant-in-Aid for Scientific Research on Innovative Areas "Organic Synthesis based on Reaction Integration" (No. 2105) from MEXT, Japan (A.F). E.Y. thanks the JSPS for a Research Fellowship for Young Scientists. Parts of the computational calculations were carried out using resources of the Research Center for Computational Science, Okazaki, Japan.

Supporting Information

Spectral data for all new compounds and results of theoretical calculations. These materials are available free of charge on J-STAGE.

References

1 a) J. R. Lakowicz, *Principles of Fluorescence Spectroscopy*, 3rd ed., Springer, **2006**. b) B. Valeur, *Molecular Fluorescence*, 3rd ed., WILEY-VCH, Weinheim, **2006**.

2 a) *The Molecular Probes Handbook*, 11th ed., Life Technologies Co., **2010**. b) L. A. Bagatolli, *Biochim. Biophys. Acta, Biomembr.* **2006**, *1758*, 1541. c) A. P. Demchenko, Y. Mély, G. Duportail, A. S. Klymchenko, *Biophys. J.* **2009**, *96*, 3461. d) G. S. Loving, M. Sainlos, B. Imperiali, *Trends Biotechnol.* **2010**, *28*, 73. e) A. S. Klymchenko, R. Kreder, *Chem. Biol.* **2014**, *21*, 97.

3 G. Weber, F. J. Farris, *Biochemistry* **1979**, *18*, 3075.

4 G. Weber, D. J. R. Laurence, *Biochem. J.* **1954**, *56*, xxxi.

5 Z. Diwu, Y. Lu, C. Zhang, D. H. Klaubert, R. P. Haugland, *Photochem. Photobiol.* **1997**, *66*, 424.

6 P. Greenspan, E. P. Mayer, S. D. Fowler, *J. Cell Biol.* **1985**,

100, 965.

7 For example, see: J. Massin, A. Charaf-Eddin, F. Appaix, Y. Bretonnière, D. Jacquemin, B. van der Sanden, C. Monnereau, C. Andraud, *Chem. Sci.* **2013**, *4*, 2833.

8 E. Yamaguchi, C. Wang, A. Fukazawa, M. Taki, Y. Sato, T. Sasaki, M. Ueda, N. Sasaki, T. Higashiyama, S. Yamaguchi, *Angew. Chem., Int. Ed.* **2015**, *54*, 4539.

9 For recent reviews for phosphole, see: a) F. Mathey, *Angew. Chem., Int. Ed.* **2003**, *42*, 1578. b) M. Hissler, P. W. Dyer, R. Réau, *Coord. Chem. Rev.* **2003**, *244*, 1. c) T. Baumgartner, R. Réau, *Chem. Rev.* **2006**, *106*, 4681. d) J. Crassous, R. Réau, *Dalton Trans.* **2008**, 6865. e) Y. Matano, H. Imahori, *Org. Biomol. Chem.* **2009**, *7*, 1258. f) A. Fukazawa, S. Yamaguchi, *Chem.—Asian J.* **2009**, *4*, 1386. g) Y. Ren, T. Baumgartner, *Dalton Trans.* **2012**, *41*, 7792. h) T. Baumgartner, *Acc. Chem. Res.* **2014**, *47*, 1613. i) M. Stolar, T. Baumgartner, *Chem.—Asian J.* **2014**, *9*, 1212.

10 T. Butters, W. Winter, *Chem. Ber.* **1984**, *117*, 990.

11 A. Fukazawa, Y. Ichihashi, Y. Kosaka, S. Yamaguchi, *Chem.—Asian J.* **2009**, *4*, 1729.

12 a) T. Sanji, K. Shiraishi, T. Kashiwabara, M. Tanaka, *Org. Lett.* **2008**, *10*, 2689. b) H. Tsuji, K. Sato, L. Ilies, Y. Itoh, Y. Sato, E. Nakamura, *Org. Lett.* **2008**, *10*, 2263. c) Y.-R. Chen, W.-L. Duan, *J. Am. Chem. Soc.* **2013**, *135*, 16754. d) Y. Unoh, K. Hirano, T. Satoh, M. Miura, *Angew. Chem., Int. Ed.* **2013**, *52*, 12975. e) B. Wu, M. Santra, N. Yoshikai, *Angew. Chem., Int. Ed.* **2014**, *53*, 7543.

13 F. Bu, E. Wang, Q. Peng, R. Hu, A. Qin, Z. Zhao, B. Z. Tang, *Chem.—Eur. J.* **2015**, *21*, 4440.

14 a) Y. Hong, J. W. Y. Lam, B. Z. Tang, *Chem. Commun.* **2009**, 4332. b) Y. Hong, J. W. Y. Lam, B. Z. Tang, *Chem. Soc. Rev.* **2011**, *40*, 5361. c) S. Yamaguchi, T. Endo, M. Uchida, T. Izumizawa, K. Furukawa, K. Tamao, *Chem.—Eur. J.* **2000**, *6*, 1683.

15 A. Fukazawa, Y. Ichihashi, S. Yamaguchi, *New J. Chem.* **2010**, *34*, 1537.

16 For the relationship between structure and fluorescent properties of 2-electron-donating group substituted benzophospholes, see: Y. Hayashi, Y. Matano, K. Suda, Y. Kimura, Y. Nakao, H. Imahori, *Chem.—Eur. J.* **2012**, *18*, 15972.

17 Compound **2a** in a poly(methyl methacrylate) (PMMA) matrix displayed a high Φ_F value of 0.72. Moreover, compound **2a** exhibited a higher Φ_F value at 77 K than that at room temperature ($\Phi_F = 0.81$ and 0.053, respectively). These increments of the Φ_F value in the PMMA matrix and at low temperature is likely due to the suppression of the rotational vibration of the substituents. See Figures S4 and S5, and Table S1 for details.

18 A. E. Reed, R. B. Weinstock, F. Weinhold, *J. Chem. Phys.* **1985**, *83*, 735.

19 J. Tomasi, B. Mennucci, R. Cammi, *Chem. Rev.* **2005**, *105*, 2999.

20 a) G. W. Robinson, R. P. Frosch, *J. Chem. Phys.* **1963**, *38*, 1187. b) K. F. Freed, J. Jortner, *J. Chem. Phys.* **1970**, *52*, 6272.

21 G.-Q. Li, Y. Yamamoto, N. Miyaura, *Tetrahedron* **2011**, *67*, 6804.

22 G. M. Sheldrick, *Acta Crystallogr., Sect. A* **2008**, *64*, 112.

23 T. Gruene, H. W. Hahn, A. V. Luebben, F. Meilleurb, G. M. Sheldrick, *J. Appl. Crystallogr.* **2014**, *47*, 462.

24 M. J. Frisch, G. W. Trucks, H. B. Schlegel, G. E. Scuseria, M. A. Robb, J. R. Cheeseman, G. Scalmani, V. Barone, B. Mennucci, G. A. Petersson, H. Nakatsuji, M. Caricato, X. Li, H. P. Hratchian, A. F. Izmaylov, J. Bloino, G. Zheng, J. L. Sonnenberg, M. Hada, M. Ehara, K. Toyota, R. Fukuda, J. Hasegawa, M. Ishida, T. Nakajima, Y. Honda, O. Kitao, H. Nakai, T. Vreven, J. A. Montgomery, Jr., J. E. Peralta, F. Ogliaro, M. Bearpark, J. J. Heyd, E. Brothers, K. N. Kudin, V. N. Staroverov, R. Kobayashi, J. Normand, K. Raghavachari, A. Rendell, J. C. Burant, S. S. Iyengar, J. Tomasi, M. Cossi, N. Rega, J. M. Millam, M. Klene, J. E. Knox, J. B. Cross, V. Bakken, C. Adamo, J. Jaramillo, R. Gomperts, R. E. Stratmann, O. Yazyev, A. J. Austin, R. Cammi, C. Pomelli, J. W. Ochterski, R. L. Martin, K. Morokuma, V. G. Zakrzewski, G. A. Voth, P. Salvador, J. J. Dannenberg, S. Dapprich, A. D. Daniels, Ö. Farkas, J. B. Foresman, J. V. Ortiz, J. Cioslowski, D. J. Fox, *Gaussian 09 (Revision C.01)*, Gaussian, Inc., Wallingford CT, **2009**.